Front. Phys. 13(5), 136104 (2018)
https://doi.org/10.1007/s11467-018-0774-2

RESEARCH ARTICLE

High-pressure polymorphs of $LiPN_2$: A first-principles study

Jian Lv[1], Xin Yang[2], Dan Xu[2†], Yu-Xin Huang[3], Hong-Bo Wang[2‡], Hui Wang[2]

[1] *College of Materials Science and Engineering, Jilin University, Changchun 130012, China*
[2] *State Key Lab of Superhard Materials, College of Physics, Jilin University, Changchun 130012, China*
[3] *College of Basic Science, Changchun University of Technology, Changchun 130012, China*
Corresponding authors. E-mail: †xudan@jlu.edu.cn; ‡whb2477@jlu.edu.cn
Received January 4, 2018; accepted March 6, 2018

In this work, high-pressure phase behavior of $LiPN_2$ within 0–300 GPa was studied by using an unbiased structure searching method in combination with first-principles calculations. Three pressure-induced phase transitions were predicted, as tI16 → hR4 → cF64 → oP8 at 44, 136, and 259 GPa, respectively. The six-fold coordination environments were found for all high-pressure polymorphs, which are substantially different from the four-fold coordination environments observed in the tI16 structure. The hR4 and cF64 structures consist of close-packed PN_6 and LiN_6 octahedra connected by edge-sharing, whereas the oP8 structure is built up from edge- and face-sharing PN_6 and LiN_6 octahedra with N lying in the center of the trigonal prisms. The electronic structure analysis reveals that $LiPN_2$ is a semiconductor within the pressure range studied and P-N and Li-N bonds are covalent and ionic, respectively. The results obtained are expected to provide insight and guidance for future experiments on $LiPN_2$ and other alkali metal nitridophosphates.

Keywords lithium nitridophosphates, phase transition, high pressure, first principles

PACS numbers 61.50.Ah, 61.66.Fn

1 Introduction

In recent years, lithium nitridophosphates have attracted considerable attention for their structural diversity and potential use in lithium ion conductors [1, 2]. To date, five lithium nitridophosphates were described in the literature; negatively charged PN_4 tetrahedra occur as characteristic building units for all of them. To be specific, isolated PN_4 tetrahedra were found in Li_7PN_4 [3], while corner-shared PN_4 tetrahedra were reported for the others. Depending on the degree of condensation of PN_4 tetrahedra, various different linking patterns occur, *i.e.*, $[P_3N_9]^{12-}$ *dreier*-rings in $Li_{12}P_3N_9$ [1], $[P_6N_{16}]^{18-}$ tricyclic ring in $Li_{18}P_6N_{16}$ [4], $[P_4N_{10}]^{10-}$ cage in $Li_{l0}P_4N_{10}$ [5], $[PN_3]^{4-}$ *zweier*-chains in Li_4PN_3 (a high-pressure polymorph of $Li_{12}P_3N_9$) [1], and $[PN_2]^{1-}$ three-dimensional network in $LiPN_2$ [3]. The conductivities observed in $LiPN_2$ and Li_7PN_4 are comparable to that of other ternary lithium nitrides, such as Li_3AlN_2, which indicates that they are potential lithium ion conductors [3].

$LiPN_2$ can be synthesized by performing reaction of the binary nitrides P_3N_5 and Li_3N at high temperatures [3]. Preliminary investigation suggested that it adopts the β-cristobalite type structure [6]. In a subsequent experimental study [3], more accurate structural information was obtained by performing X-ray diffraction analysis on $LiPN_2$ having single phase. It revealed that the atomic arrangement analogous to β-cristobalite could also be derived from the chalcopyrite type of structure. However, compared to β-cristobalite, all PN_4-tetrahedra are rotated about their $\bar{4}$ axes. In 2007, a systematic crystal-chemical analysis proved that this compound occupies an intermediate position between the ideal structures of β-cristobalite and chalcopyrite and that its valence band differs radically from the typical valence band of chalcopyrite crystals [7]. Lattice dynamics and elastic properties of $LiPN_2$ have also been studied through *ab initio* calculations and the strong covalent bond between P and N atoms was found to play a key role in determining those properties [8].

High pressure can significantly promote the condensation of PN_4 tetrahedra for ternary phosphorus ni-

trides. A good example was observed in $Li_{12}P_3N_9$ where the $[P_3N_9]^{12-}$ *dreier*-rings were superseded by $[PN_3]^{4-}$ *zweier*-chains at pressures above 6 GPa, leading to the formation of Li_4PN_3 [1]. High pressure is also a unique tool to create higher-coordination polyhedra from PN_4 tetrahedra, for instance, PN_5 bipyramids appear at 14 GPa in g-P_4N_6(NH), a high-pressure polymorph of P_4N_6(NH) [9]. As the element combination P/N is isoelectronic with Si/O, the structural variety of ternary phosphorus nitrides is expected to be similar to that of silicates. SiO_6 octahedra have been widely observed in the high-pressure polymorphs of silicates. However, PN_6 octahedra have not yet been identified experimentally for any ternary phosphorus nitrides, despite the fact that these have long been predicted in the spinel-type BeP_2N_4 that would be stable at pressures above 23 GPa [10]. It is therefore of great interest to investigate the high-pressure polymorphs and the coordination chemistry of this compound class.

Here, we report an extensive study on the high-pressure structures of $LiPN_2$ in the pressure range of 0-300 GPa *via* our in-house-developed swarm-intelligence-based CALYPSO method for crystal structure prediction. Three pressure-induced phase transitions were predicted for $LiPN_2$, as tI16 → hR4 → cF64 → oP8 at 44, 136 and 259 GPa, respectively. All the high-pressure polymorphs had six-fold coordination environments. The analysis of electronic structure reveals that $LiPN_2$ is a semiconductor at the pressures studied and the P-N and Li-N bonds have covalent and ionic nature, respectively.

2 Computational details

We used the CALYPSO method [11, 12] to search for the high-pressure polymorphs; this method has been widely used in crystal structure prediction [13–16]. Structure searches with system sizes ranging from two to four formulas per simulation cell were performed for pressure values of 50, 100, 200, and 300 GPa. The total energy calculations and local structural relaxations were carried out by using the density functional theory as implemented in the VASP code [17]. The projector augmented wave potentials [18] with $1s^2 2s^1$, $3s^2 3p^3$, and $2s^2 2p^3$ electrons as valence were adopted for Li, P, and N, respectively. The cutoff energy (900 eV) for the expansion of the wave function into plane waves and Monkhorst-Pack k point meshes [19] with a grid of 0.025 $Å^{-1}$ were chosen to ensure that enthalpy calculations were well converged to the level of 1 meV/atom. The phonon density of states and crystal orbital Hamilton population were calculated by PHONOPY [20] and LOBSTER software [21]. The crystal structures were plotted by VESTA code [22].

3 Results and discussion

The enthalpies of the most energetically competitive structures of $LiPN_2$ at pressures up to 300 GPa are shown in Fig. 1. For low-pressure values, the tI16 structure was found to be most favorable, which is in agreement with the experimental observation. The enthalpy of the tP16 structure is only 6 meV/$LiPN_2$ higher at 0 GPa, and keeps close to the tI16 structure under a wide range of pressure, indicating that it might be metastable. The two structures are isoenthalpic up to 72 GPa, however, before that the hR4 structure becomes most stable at 44 GPa. Notably, the tI16 → hR4 transition in $LiPN_2$ differs from what we found in the compressed $CuPN_2$ [23]. To be specific, $LiPN_2$ and $CuPN_2$ adopt identical ground state tI16 structure but different high-pressure hR4 structures. The hR4 and cF64 structures are energetically nearly degenerated in a wide pressure range of 110–300 GPa. At pressures above 136 GPa, the enthalpy of cF64 lowers consistently by 10 meV/$LiPN_2$, indicating the occurrence of a hR4 → cF64 phase transition. Since the energy cutoff and k-point sampling were chosen such that the enthalpies would converge to within ~1 meV/atom across the pressure range studied, such an enthalpy difference is within the precision of our calculations. At pressures above 259 GPa, oP8 becomes the most stable structure and remains so until at least to 300 GPa. In addition, the hP8 and oC16 structures were found to lie within 200 meV/$LiPN_2$ of the most favorable high-pressure polymorphs within several different pressure ranges.

As $LiPN_2$ is composed of light elements, the zero-point

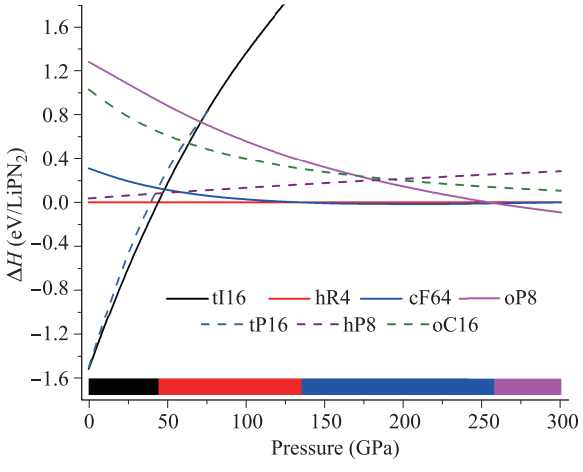

Fig. 1 Calculated enthalpies per formula unit (relative to hR4 structure) of the high-pressure phases for $LiPN_2$; the stable regime is indicated by colored bars at the bottom of the figure.

energy (ZPE) correction would be expected to affect the relative stability of the energetically competing structures, such as tI16 and tP16, and hR4 and cF64. The ZPE of tI16 is lower than that of tP16 by 47 meV/$LiPN_2$, which supports the fact that tI16 is the thermodynamic ground state at ambient pressure. The difference in the ZPE of hR4 and cF64 is less than 2 meV within the pressure range of 120–160 GPa and therefore cannot alter their relative stability. The phase transitions were found to be delayed by ZPE. However, the pressure shifts are within 8 GPa. Overall, inclusion of the ZPE correction had a negligible effect on the phase sequence. The finite temperature effects were further estimated based on the harmonic approximation. The pressure shifts increase with increasing temperature with pressure changes reaching 11–14 GPa at 1000 K.

In the tI16 structure (space group: I-42d; $Z = 4$), P and N atoms form a three-dimensional net of corner-sharing PN_4 tetrahedra, while Li cations occupy positions which are nearly tetrahedrally coordinated by N atoms (Fig. 2a). At ambient pressure, the structural parameters in tetragonal unit cell are: $a = 4.571$ Å and $c = 7.293$ Å, with Li 4b (0, 0, 0.5), P 4b (0, 0, 0), and N 8d (0.832, 0.25, 0.125). Our theoretical results basically agree with the experimental values of $a = 4.575$ Å and $c = 7.118$ Å [3]. The P-N-P angle is 124.63° and the PN_4 tetrahedra deviate slightly from the regular tetrahedron with dihedral angles splitting into 68.72° and 74.09°. In view of the fact that tI16 is a β-cristobalite-related structure, it is no surprise that our predicted metastable tP16 is an α-cristobalite-related structure with space group $P4_32_12$ and $Z = 4$. At ambient pressure, the structural parameters are $a = 4.871$ Å and $c = 6.502$ Å, with Li 4a (0.200, 0.200, 0), P 4a (0.812, 0.812, 0), and N 8b (0.725, 0.646, 0.791). The P-N-P angle is 130.48° and the PN_4 tetrahedra are distorted with dihedral angles ranging from 69.11° to 72.28°. Notably, the PN_4-tetrahedra networks of both structures can be derived from the Fd-3m unit cell of the well-known $C9$ structure originally proposed by Wyckoff for high-cristobalite [24]. The volume of tI16 is about 1% smaller than that of tP16 at 0 GPa, however, the relation is reversed at a pressure of 44 GPa, which illustrates the increasing role of internal energy in stabilizing the former with respect to the latter under compression.

The tI16 and hR4 structures are isoenthalpic at 44 GPa, where the volume of the latter is 15% less than the former. Pressure lowers the enthalpy by $\Delta H = \int \Delta V \mathrm{d}P$, thus favoring the stability of hR4 at increasing pressure. In a pressure-induced first-order phase transition, a large volume collapse is usually related to the increase of coordination numbers. In hR4, an important structural feature observed is that all atoms (Li, P and N) are six-fold coordinated, forming octahedra sharing eight edges with one another (Fig. 2b), which significantly differs from the four-fold coordination environments observed in the low-pressure tI16 structure. At 60 GPa, structural parameters of hR4 (space group R-3m; $Z = 1$) in the hexagonal cell are: $a = 2.553$ Å and $c = 13.274$ Å, with Li 3b (0, 0, 0.5), P 3a (0, 0, 0), and N 6c (0, 0, 0.262). The PN_6 octahedron deviates slightly from the regular octahedron with dihedral angles splitting into 111.24° and 107.64°. The hR4 is isostructural with the second high-pressure phase of $CuPN_2$ [23] that also adopts the tI16 structure at ambient pressure. The first high-pressure phase of $CuPN_2$ is a different rhombohedral structure with two-coordinated Cu atoms, which does not appear in the phase sequence of $LiPN_2$ due to the very high enthalpies. This is understandable, considering that $CuPN_2$ is a double nitride consisting of covalent Cu-N bond that can stabilize a low-coordination environment, however, Li cations have to fill the octahedral voids for lowering the volume. The tI16 → hR4 phase transition has also been predicted for $MgSiN_2$ [25] (at 25 GPa) isoelectronic system of $LiPN_2$.

In the hR4 → cF64 phase transition at 136 GPa, the volume decreases slightly by 0.35%, significantly less than that in the first phase transition, which is attributed to the similarity of the six-fold coordination environments of the two structures, as shown in Fig. 2. A major

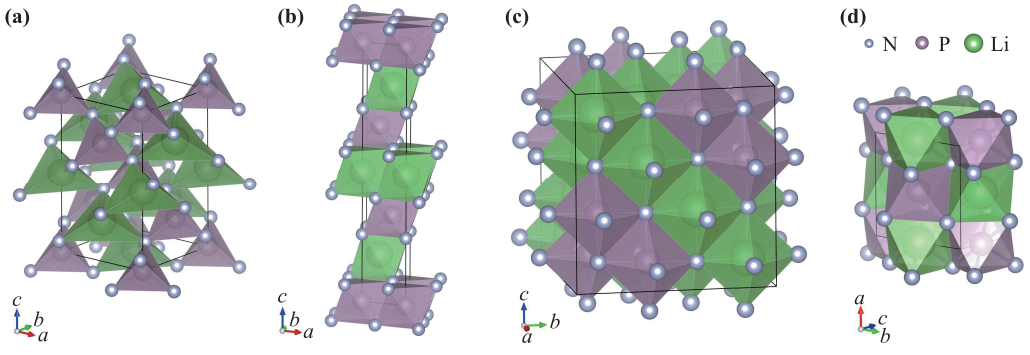

Fig. 2 Crystal structure of $LiPN_2$, **(a)** tI16, **(b)** hR4, **(c)** cF64, and **(d)** oP8 structures.

structural difference between the hR4 and cF64 structures is that PN_6 octahedra form two-dimensional layers in the former while a three-dimensional network is formed in the latter. At 160 GPa, structural parameters of cF64 (space group: Fd-$3m$; $Z = 16$) in common unit cell are: $a = 6.913$ Å, with Li 16c (0.125, 0.125, 0.125), P 16d (0.125, 0.375, 0.875), and N 32e (0.868, 0.868, 0.868). The PN_6 octahedron in the cubic cF64 is also lightly distorted in comparison to the regular one with dihedral angles splitting into 110.84° and 108.07°. A volume collapse of 2% was found in the cF64 → oP8 phase transition at 259 GPa, which is about six times that in the hR4 → cF64 phase transition. Though the coordination number remains six, the manner of connections of PN_6 and LiN_6 octahedra is much different: Except for sharing six edges, every octahedron shares two faces with others (Fig. 2d). As a result, the local coordination environment of N atom is a trigonal prism instead of an octahedron. The presence of shared faces in oP8 increases its density over the cF64 structure. At 280 GPa, structural parameters of oP8 (space group $Pnnm$; $Z = 2$) in unit cell are: $a = 3.853$ Å, $b = 3.931$ Å, and $c = 2.345$ Å, with Li 2c (0, 0.5, 0), P 2b (0, 0, 0.5), and N 4g (0.347, 0.841, 0). In comparison with cF64, the PN_6 octahedron of oP8 is more distorted with dihedral angles ranging from 107.44° to 113.20°.

The dynamical stability of a crystalline structure requires the eigen frequencies of its lattice vibrations be real for all wave vectors in the Brillouin zone. The phonon frequencies were calculated for each of the five structures at several different pressures within the phase stable regime, and the absence of imaginary frequency indicates that those structures are dynamically stable. The phonon density of states (PDOS) of the five structures, which were projected on Li, P, and N atoms, are shown in Fig. 3. No big differences have been found between the tI16 and tP16 structures at 0 GPa except for a small disparity in the frequency of the last two peaks that related to the intramolecular vibrational modes of PN_4 tetrahedra. This disparity seems to be one of the reasons for the tP16 structure having larger ZPE than the tI16 structure. For the hR4 structure, gaps between different peaks become unclear and PDOS of Li component are more dispersive in comparison with the tI16/tP16 structure. This is understandable, considering that interactions between the edge-shared octahedra should be stronger than that of the corner-shared tetrahedra. However, as the P-N bond lengths increase with increasing coordination numbers in the tI16 → hR4 phase transition, the last peaks shift slightly to lower frequencies. As shown in Fig. 3(c–e), the vibrational frequencies of the three six-fold coordinated high-pressure polymorphs increase generally with increasing pressure and the Li component contributes more to the high-frequencies as

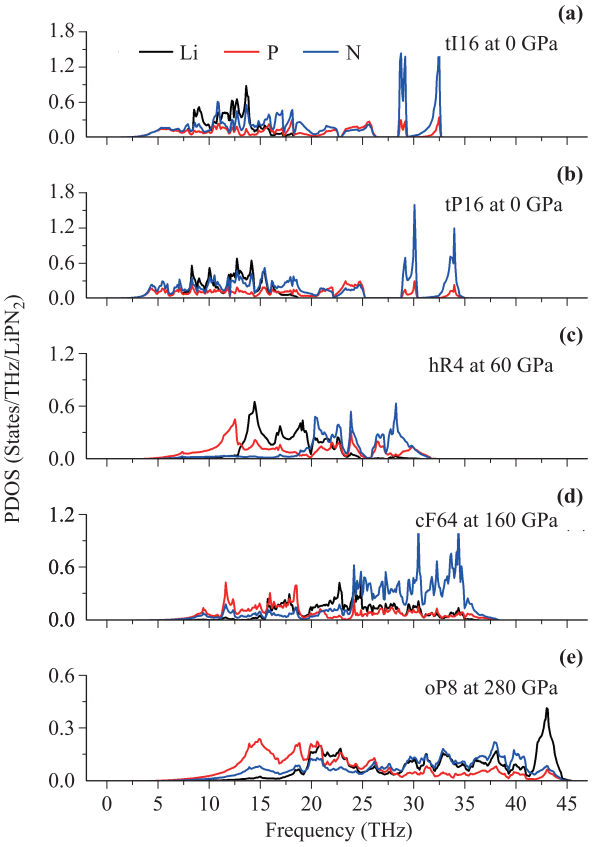

Fig. 3 Atom-projected PDOS of tI16 **(a)**, tP16 **(b)**, hR4 **(c)**, cF64 **(d)**, and oP8 **(e)** structures.

a result of its small atomic mass.

The electronic density of states (DOS) curves of the four energetically stable structures are shown in Fig. 4. The existence of energy gaps (E_g) indicates that $LiPN_2$ is a semiconductor in the whole pressure range studied. For each individual structure, E_g decreases with increasing pressure, however, in the three phase transitions E_g varies in a series of decrease → increase → decrease. The cF64 structure possesses the largest E_g among the four structures. E_g of 5.62 eV predicted for this structure at 160 GPa is about 46 %, 57 %, and 33 % larger than that of tI16 at 0 GPa, hR4 at 60 GPa and oP8 at 280 GPa, respectively. Notably, large gaps also appear in the valence bands of this structure, *e.g.* the one at around 14 eV. The cubic (Oh) symmetry seems to favor large separations between subbands that originate from the hybridization of the s and p states. Therefore, it is no surprise that a large energy gap is formed between the bonding and antibonding states. The energy gap of a semiconductor usually decreases with increasing pressure, especially in a first order structural phase transition with a sizable volume collapse. In our previous work on $CuPN_2$, an abnormal increase of the energy gap was predicted in an

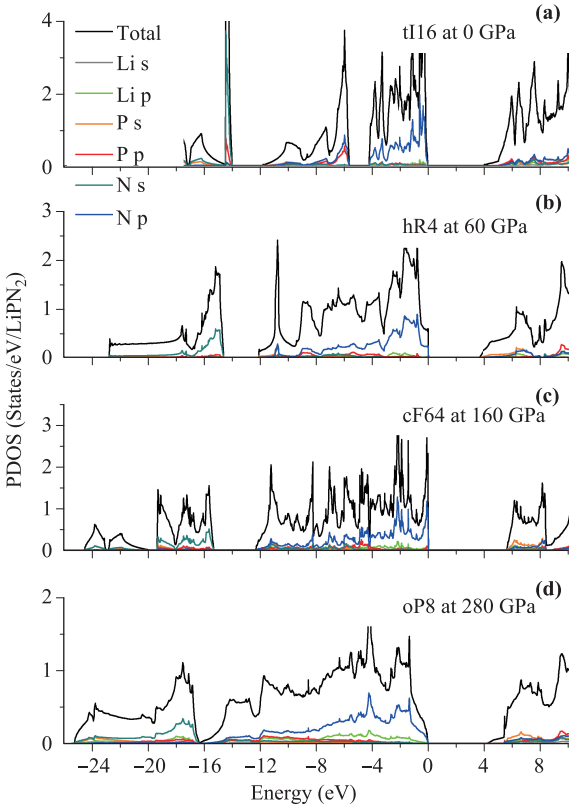

Fig. 4 Total and partial (or orbital-projected) DOS of tI16 **(a)**, hR4 **(b)**, cF64 **(c)**, and oP8 **(d)** structures.

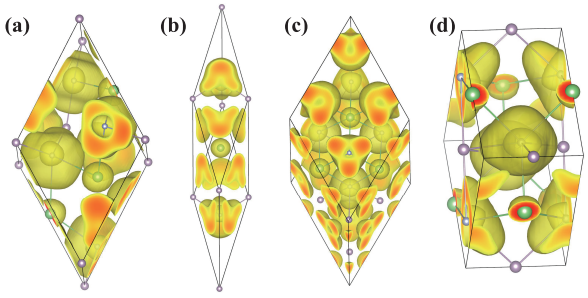

Fig. 5 ELF of tI16 structure at 0 GPa **(a)**, hR4 structure at 60 GPa **(b)**, cF64 structure at 160 GPa **(c)**, and oP8 structure at 280 GPa **(d)** with isosurface of 0.7.

isosymmetric hexagonal → hexagonal transition at about 120 GPa, however, it was mainly attributed to the significant increase of Cu-N distance. In the hR4 → cF64 transition of $LiPN_2$, the volume collapse is only about 0.35 % and the Li-N and P-N distances are nearly unchanged which further supports the change of the lattice symmetry to be the origin of the abnormal increase of the energy gap.

The electron localization function (ELF) is useful tool for distinguishing between different bonding situations in solids. As shown in Fig. 5, the ELF plots indicate that a large number of electrons are present at the N site, and directional bonding characters are clearly seen from the non-spherical distribution for all of them. The large ELF value along the N-P direction indicates a covalent interaction. In comparison with the N-P direction, the isosurface along the N-Li direction is nearer to N atom and the isosurface at the Li site is nearly spherically symmetric indicating an ionic interaction between Li and N atoms. To estimate of the net strength of the bonding of N-P and N-Li pairs, we further calculated the integrated crystal orbital Hamilton population (ICOHP). For the four-fold coordinated tI16 structure at 0 GPa, ICOHP of N-P and N-Li pairs are about −8.2 and −2.9 eV, respectively, which are both higher than those of the three high-pressure polymorphs. This is understandable considering that the high-pressure polymorphs are six-fold coordinated and there are more bonds to share the centered atom. It is found that the ICOHP of N-P pair is inversely proportional to bonding length, for instance, averaged values of −6.5 and −7.0 eV were found in hR4 at 60 GPa and cF64 at 160 GPa with N-P distances of 1.75 and 1.68 Å, respectively. This trend further supports the covalent bonding nature of the N-P bonds. However, similar trend was absent for N-Li pairs, which can be attributed to its ionic bonding nature.

4 Summary

In the present study, we explored the phase stability, structural, and electronic properties of $LiPN_2$ extensively, over a wide pressure range of 0–300 GPa by using an unbiased structure searching method in combination with first-principles calculations. Three pressure-induced phase transitions tI16 → hR4 → cF64 → oP8 were predicted at 44, 136 and 259 GPa, respectively. All of the three high-pressure polymorphs have six-fold coordination environment, which is substantially different from the four-fold coordinated tI16 structure. The hR4 and cF64 structures consist of close-packed PN_6 and LiN_6 octahedra connected by edge-sharing, whereas, the oP8 structure is built up from edge- and face-sharing PN_6 and LiN_6 octahedra with N lying in the center of trigonal prisms. Phonon calculations showed that all of the three high-pressure polymorphs are dynamically stable. Electronic property analysis reveals that $LiPN_2$ is a semiconductor within the studied pressure range, and P-N and Li-N bonds are covalent and ionic, respectively. The current results provide new insight and guidance for further studying alkali metal nitridophosphates at high pressures.

Acknowledgements The authors acknowledge funding support from the National Natural Science Foundation of China (Grant

Nos. 11474128 and 11534003), Science Challenge Project (Grant No. TZ2016001), National Key Research and Development Program of China (Grant Nos. 2016YFB0201200, 2016YFB0201201, and 2016YFB0201204), and Program for JLU Science and Technology Innovative Research Team. Parts of the calculations were performed in the high-performance computing center of Jilin University.

References

1. E. M. Bertschler, R. Niklaus, and W. Schnick, $Li_{12}P_3N_9$ with non-condensed $[P_3N_9]^{12-}$-rings and its high-pressure polymorph Li_4PN_3 with infinite chains of PN_4^- tetrahedra, *Chemistry* 23(40), 9592 (2017)
2. A. Al-Qawasmeh and N. A. W. Holzwarth, $Li_{14}P_2O_3N_6$ and Li_7PN_4: Computational study of two nitrogen rich crystalline LiPON electrolyte materials, *J. Power Sources* 364, 410 (2017)
3. W. Schnick and J. Luecke, Lithium ion conductivity of $LiPN_2$ and Li_7PN_4, *Solid State Ion.* 38(3–4), 271 (1990)
4. E. M. Bertschler, C. Dietrich, J. Janek, and W. Schnick, $Li_{18}P_6N_{16}$ — A lithium nitridophosphate with unprecedented tricyclic $[P_6N_{16}]^{18-}$ Ions, *Chemistry* 23(9), 2185 (2017)
5. W. Schnick and U. Berger, $Li_{10}P_4N_{10}$ — A lithium phosphorus(V) nitride containing the new complex anion $[P_4N_{10}]^{10-}$, *Angew. Chem. Int. Ed. Engl.* 30(7), 830 (1991)
6. R. Marchand, P. L'Haridon, and Y. Laurent, Etude cristallochimique de $LiPN_2$: Une structure derivée de la cristobalite, *J. Solid State Chem.* 43(2), 126 (1982)
7. Y. M. Basalaev, Y. N. Zhuravlev, V. S. Permina, and A. S. Poplavnoi, $LiPN_2$ and $NaPN_2$ crystals: Structural features and chemical bonding, *J. Struct. Chem.* 48(6), 996 (2007)
8. A. V. Kosobutsky, Lattice dynamics and elastic properties of $LiPN_2$ and $NaPN_2$, *J. Phys. Condens. Matter* 21(40), 405404 (2009)
9. D. Baumann and W. Schnick, Pentacoordinate phosphorus in a high-pressure polymorph of phosphorus nitride imide $P_4N_6(NH)$, *Angew. Chem. Int. Ed.* 53(52), 14490 (2014)
10. F. J. Pucher, S. R. Römer, F. W. Karau, and W. Schnick, Phenakite-type BeP_2N_4 — A possible precursor for a new hard spinel-type material, *Chemistry* 16(24), 7208 (2010)
11. Y. Wang, J. Lv, L. Zhu, and Y. Ma, Crystal structure prediction via particle-swarm optimization, *Phys. Rev. B* 82(9), 094116 (2010)
12. Y. Wang, J. Lv, L. Zhu, and Y. Ma, CALYPSO: A method for crystal structure prediction, *Comput. Phys. Commun.* 183(10), 2063 (2012)
13. Y. Wang and Y. Ma, Perspective: Crystal structure prediction at high pressures, *J. Chem. Phys.* 140(4), 040901 (2014)
14. Y. Wang, J. Lv, L. Zhu, S. Lu, K. Yin, Q. Li, H. Wang, L. Zhang, and Y. Ma, Materials discovery via CALYPSO methodology, *J. Phys.: Condens. Matter* 27(20), 203203 (2015)
15. H. Wang, Y. Wang, J. Lv, Q. Li, L. Zhang, and Y. Ma, CALYPSO structure prediction method and its wide application, *Comput. Mater. Sci.* 112 (Part B), 406 (2016)
16. L. Zhang, Y. Wang, J. Lv, and Y. Ma, Materials discovery at high pressures, *Nat. Rev. Mater.* 2(4), 17005 (2017)
17. G. Kresse and J. Furthmüller, Efficient iterative schemes for ab initio total-energy calculations using a plane-wave basis set, *Phys. Rev. B* 54(16), 11169 (1996)
18. P. E. Blöchl, Projector augmented-wave method, *Phys. Rev. B* 50(24), 17953 (1994)
19. H. J. Monkhorst and J. D. Pack, Special points for Brillouin-zone integrations, *Phys. Rev. B* 13(12), 5188 (1976)
20. A. Togo, F. Oba, and I. Tanaka, First-principles calculations of the ferroelastic transition between rutile-type and $CaCl_2$-type SiO_2 at high pressures, *Phys. Rev. B* 78(13), 134106 (2008)
21. S. Maintz, V. L. Deringer, A. L. Tchougréeff, and R. Dronskowski, LOBSTER: A tool to extract chemical bonding from plane-wave based DFT, *J. Comput. Chem.* 37(11), 1030 (2016)
22. K. Momma and F. Izumi, VESTA 3 for three-dimensional visualization of crystal, volumetric and morphology data, *J. Appl. Cryst.* 44(6), 1272 (2011)
23. D. Xu and B. Li, Exotic high-pressure behavior of double nitride $CuPN_2$ (unpublished)
24. R. W. G. Wyckoff, Crystal structure of high temperature cristobalite, *Am. J. Sci.* s5–9(54), 448 (1925)
25. M. Råsander and M. A. Moram, Electronic structure of the high and low pressure polymorphs of $MgSiN_2$, *Mater. Res. Express* 3(8), 085902 (2016)